Utilizing Near Edge X-ray Absorption Fine Structure to Probe Interfacial Issues in Photolithography

Joseph L. Lenhart[1,3], Daniel A. Fischer[1], Sharadha Sambasivan[1], Eric K. Lin[1], Christopher L. Soles[1], Ronald L. Jones[1], Wen-li Wu[1], Dario L. Goldfarb[2], Marie Angelopolous[2]

[1]National Institute of Standards and Technology, Gaithersburg, MD
[2]IBM, Yorktown Heights, NY
[3]Current address: Sandia National Laboratories, Albuquerque, NM

Control of the shape, critical dimension (CD), and roughness is critical for the fabrication of sub 100 nm features, where the CD and roughness budget are approaching the molecular dimension of the resist polymers[1]. Here we utilize near edge X-ray absorption fine structure (NEXAFS) to provide detailed chemical insight into two interfacial problems facing sub-100 nm patterning. First, chemically amplified photo-resists are prone to surface phenomenon, which causes deviations in the pattern profile near the interface. Striking examples include T-topping, closure, footing, and undercutting. NEXAFS was used to illustrate that the surface extent of deprotection in a model resist film can be different than the bulk deprotection. Second, line edge roughness becomes increasingly critical with shrinking patterns, and may be intimately related to the line edge deprotection profile. A NEXAFS technique to surface depth profile for compositional gradients is described with the potential to provide detailed chemical information about the resist line edge.

Introduction

Control of the shape, critical dimension (CD), and line edge roughness (LER) is essential for the fabrication of sub-100 nm features, where the CD and roughness budget are approaching the molecular dimension of the resist polymers (1). With shrinking pattern sizes the performance of chemically amplified photo-resists will become increasingly prone to interfacial or surface phenomena, which cause deviations in the pattern profile near the interface. Striking examples include T-topping, closure, footing, and undercutting. In addition, line edge roughness that is acceptable for current patterning dimensions will be unacceptable in smaller patterns. It is therefore important to develop and utilize new tools to probe the interfacial composition and structure of photoresist films. Here we demonstrate the utility of NEXAFS for providing information about lithographic interfaces, focusing initially on the T-topping / closure issue and probing the extent of deprotection at the resist surface. Second, the NEXAFS technique is described to surface depth profile in a model line edge region offering the potential to provide detailed chemical information about surface compositional gradients.

Experimental

Materials and Methods. The model resist solution was composed of 0.7 g of protected polymer poly(tertbutyloxy- carbonyloxy- styrene, $M_{n,r}$=15,000) (PBOCSt) mixed with 0.035 g (0.05 mass fraction of PFOS relative to the polymer) of the photo acid generator, bis(p-tert-butylphenyl) iodonium perfluorooctanesulfonate (PFOS). This mixture was dissolved in 20 mL of propylene glycol methyl ether acetate (PGMEA). The resist solution was spun cast onto silicon wafers at 1500 rpm for 60 s and then post apply baked (PAB) for 60 s at 100 ^{o}C. The PBOCSt / PFOS films were blanket exposed to ultra-violet radiation from a broadband source with wavelengths ranging between (220 and 260) nm with a total dose of 500 mJ/cm^2. After exposure the films were post exposure baked (PEB) at 100 ^{o}C for 2 min. Polyhydroxystyrene, $M_{n,r}$=5,000, (PHS) / PFOS films were made according to the same procedures described above.

NEXAFS. NEXAFS measurements were conducted at the U7A beamline of the National Synchrotron Light Source at Brookhaven National Laboratory. A monochromator with a 600 line/mm grating, providing ± 0.15 eV resolution,

was used for all the NEXAFS spectra. The monochromator energy scale was calibrated by the carbon K-edge π^* transition of graphite at 285.35 eV. All the spectra were recorded at room temperature in the NIST – Dow material characterization chamber (2) at 10^{-6} Pa. The spectra were normalized to the incident beam intensity, I_0, by collecting the total electron yield intensity from a gold coated 90 % transmitting grid placed in the incoming X-ray beam path. The carbon fluorescence-yield intensity was measured utilizing a differentially pumped, UHV compatible proportional counter filled with 200 Torr of P-90 (90% methane, 10% argon) in an energy dispersive mode (3) to reduce background fluorescence from other elements. Surface sensitive partial electron yield measurements were made (probe depth of approximately 1 to 6 nm) by applying a negative bias on the entrance grid of the channeltron electron detector. For the carbon K-edge spectra (260 to 330) eV, the electron yield detector was set with a negative bias of 150 eV. The spectra were collected with the incident beam at the magic angle (54.7^o) relative to the sample in order to remove any polarization dependence. For the NEXAFS spectra in this paper the experimental standard uncertainty in the peak position is similar to the grating resolution of ± 0.15 eV. The relative uncertainty in the NEXAFS intensity is less than ± 5% and was determined by multiple scans on a sample.

For some experiments, bilayer samples of PBOCSt and PHS were spun cast onto silicon wafers. The wafers were cleaned by immersion in sulfuric acid and hydrogen peroxide solution followed by a rinse in deionized water. A hydrophobic surface was generated by treating the wafers with hexamethyldisilazane (HMDS) vapor in a vacuum oven. The bottom PBOCSt layer was spun cast from solution with PGMEA and soft baked for 60 s at 130 ^{o}C. A top layer of PHS (with a 5 % mass loading of PFOS) was spun cast on PBOCSt from a solution of n-butanol. The samples were exposed to UV radiation, and post exposure baked for various times at 90 ^{o}C. After PEB, the soluble top portion of the bilayer film was removed (developed) by immersion in an aqueous 0.26 N tetra-methyl-ammonium-hydroxide solution (4,5). NEXAFS measurements were then conducted on the developed bilayer samples as a function of the electron yield detector bias. For the depth profiling measurements on the bilayer surfaces the negative bias on the electron yield detector was varied between (50 and 245) eV.

NEXAFS at the Resist Air Interface

Figure 1 shows a schematic depicting the principles of NEXAFS. The sample is exposed to tunable plane polarized, monochromatic X-ray radiation from a synchrotron light source. In these experiments, the incident radiation is

scanned over the carbon K-edge region, an energy range from (260 to 330) eV. X-rays are preferentially absorbed by the sample when the incident radiation is at the appropriate energy to allow the excitation of a core shell electron to an unoccupied molecular orbital. During electronic relaxation Auger electrons and characteristic fluorescence photons are released. The electronic relaxation processes may release more than one electron. These electrons can only escape from the top surface of the sample (1 to 8) nm. The photons have a longer escape depth of ~100 nm within the sample. Because the characteristic binding energies of carbon, nitrogen, oxygen, and fluorine core electrons are well separated in energy, NEXAFS has elemental sensitivity. In addition, due to the well-defined energy gap associated with a core shell / unoccupied orbital transition, NEXAFS is also sensitive to the bonding characteristics of the atoms (6).

Figure 1 also shows a carbon edge electron yield NEXAFS spectrum for PBOCSt. In the pre-edge region, the incident radiation is weakly absorbed by the sample. The intensity in this region, I_b, is the background signal (often from the substrate and sample, lower energy absorption edges, orbital transitions other than core level transitions, etc.). Above the carbon K edge (285 eV), the signal intensity (electron or fluorescence yield) increases when the incident radiation is strongly adsorbed by the sample. In the near edge region, the peaks represent chemical bonding structure in the sample because the emission signal increases when the incident energy is the appropriate energy to cause an electron transition from the core 1s orbital to an unoccupied molecular orbital. The absorption edge represents the ionization of the core shell electron to the continuum. The edge jump, I_j, is defined as I_s-I_b. In the post edge region the signal intensity, I_j, represents total amount of carbon (since the scan is over the carbon K-edge energy range) in the sampling volume. All the NEXAFS spectra in this paper are pre-edge jump normalized to zero by subtracting I_b from the spectrum.

Figure 2 shows the carbon edge NEXAFS spectra for the neat components used in our model resist system. The spectra are vertically offset for clarity. The top spectrum is for the protected polymer, PBOCSt. The peak at 285.0 eV reflects the π^* transition from to the carbon-carbon double bonds in the styrene ring. At 290.3 eV is a peak associated with the protective group, specifically the π^* transition of the carbon-oxygen double bond from the carbonyl group. The middle spectrum, for the PFOS photo-acid generator, also displays a sharp carbon-carbon π^* transition similar to PBOCSt. However, the broad peaks between (292.0 and 298.0) eV are due to σ^* transitions for carbon-fluorine bonds (292.0 and 298.0) eV and carbon-carbon bonds, 295.0 eV, on PFOS. The bottom spectrum is for the deprotected polymer, PHS, which also contains the strong π^* transition at 285.0 eV. Distinct peaks can be used to detect the individual resist components. For example, the peak at 290.3 eV in PBOCSt, associated with the protective group, is not present in PHS or PFOS, allowing

the direct monitoring of the de-protection reaction. Also the carbon-fluorine peaks in PFOS are not present in the other two spectra, although they may partially overlap with the carbon-carbon σ^* transition.

Figure 3 compares the electron and fluorescence yield for the PBOCSt / PFOS films after various processing conditions. By monitoring the C=O π^* transition from the carbonyl on PBOCSt, the extent of deprotection can be followed during processing. In Figure 3, the spectra are both pre- and post-edge jump normalized. The post-edge jump normalization involves dividing the pre-edge jump normalized spectra by the edge jump intensity (I_j from Figure 1). This eliminates the spectral dependence on total carbon content in the sampling volume and changes in the NEXAFS peak intensity are due to chemical changes in the system. Figure 3a shows the fluorescence yield (bulk) spectrum from the samples. A strong carbonyl peak is present in the PAB, and PAB / UV treated samples andoverlap with each other. After a 20 s PEB at 100 ^{o}C, the peak at 290.3 eV decreases, but not completely. Even after 2 min PEB, the peak at 290.3 eV is not completely gone.

Figure 3b shows the electron yield (surface) spectra for the same PBOCSt / PFOS films. After both the PAB and a PAB + UV, the C=O π^* transition at 290.3 eV is large in the electron yield (Figure 3b) indicating the polymer is still protected. However, after a short 20 s PEB at 100 ^{o}C, the carbonyl peak completely disappears in the electron yield indicating complete deprotection at the film surface. Also shown in Figure 3b is the curve for the PBOCSt / PFOS film after 2 min PEB, and a PHS / PFOS film after a PAB. These curves overlap with the PBOCSt / PFOS film after the 20 s PEB in the carbonyl region near 290.3 eV, verifying that complete surface deprotection occurs in the first 20 s of post exposure baking. Comparison of the electron yield with the fluorescence yield spectrum clearly illustrates that the surface reaction rate is faster than the bulk. In addition, the electron yield spectra exhibit strong carbon-fluorine peaks between (292 and 298) eV from the PFOS. Since these peaks are not observed in the fluorescence yield spectra, this illustrates significant PFOS segregation to the film surface. This large surface segregation of the PAG would lead to a higher acid content near the air interface and increase the deprotection reaction rate. The PFOS is present in small quantities in the bulk of the film (0.05 mass fraction of PFOS relative to polymer, 0.013 mole fraction of PFOS relative to PBOCSt monomers). At small PFOS concentration, the large carbon background from the PBOCSt polymer will dampen the contribution of the C-F peaks from PFOS. Since the C-F peaks are easily observable in the electron yield but not in the fluorescence yield, this qualitatively illustrates a strong surface enrichment of the PFOS. We are currently developing a technique to extract the surface composition quantitatively from the electron yield spectra, by using a linear combination of the pure component spectra.

In Figure 3, there were no delay times between successive processing steps: spin coat, PAB, UV exposure, PEB. However, time delays between the various steps can have a significant impact on the resultant lithographic patterns. Figure 4 shows the carbon K-edge fluorescence (Figure 4a) and electron yield (Figure 4b) spectra for a PBOCSt / PFOS film after the PAB only, and after a PAB + UV + PEB sequence. The NEXAFS spectra in Figure 4a,b are from the same sample. However, for this sample a (5 to 10) min delay time was incorporated between the UV exposure and PEB. This is called a post exposure delay (PED). In the carbon edge fluorescence yield spectra, a carbonyl peak at 290.3 eV is observed in the PAB film. After UV exposure and a 2 min PEB at 100 ^{o}C, the peak area has dramatically decreased, indicating deprotection in the bulk of the resist film (Figure 4a). In the carbon edge electron yield spectra, the peak decreases only slightly after UV exposure and PEB, indicating incomplete deprotection at the film surface (Figure 4b).

The mechanisms leading to the incomplete surface deprotection reaction due to PED have not been determined and are the focus of our current research. One possible explanation is acid neutralization in the resist film due to atmospheric contaminants. Nalamasu et al. showed that the post exposure bake delay time was critical to the performance of chemically amplified resists (7). A PED of several minutes lead to an aqueous-base insoluble residue at the resist / air interface, while longer PED times prevent the lithographic image from being developed (7). It was shown that resist performance deteriorated dramatically in basic environments, but could be improved by controlling the processing atmosphere or coating the resist with a base-neutralizing (weakly acidic) polymer layer (7). Incomplete deprotection near the resist / air interface was suggested as the cause of the insoluble residual layer (7). MacDonald et al. also showed that airborne amine contaminants degrade resist performance by leading to the formulation of a thin insoluble skin at the resist / air interface (8). Hinsberg et al. illustrated that the extent of base contamination in a resist film depends on the polymer solubility parameter, and the temperature difference between the post apply bake and the polymer glass transition (9). So, the extent of resist contamination will depend on the polymer-contaminant interaction as well as the physical and thermal properties of the resist films.

PED is considered to be a critical factor in T-topping (7,10). These experiments illustrate that a PED between (5 and 10) min can lead to incomplete surface deprotection. The PAB temperature of 100 ^{o}C for these PBOCSt / PFOS films was below the glass transition of bulk PBOCSt. By comparison to the work of Hinsberg et al. (9) this would lead to an uptake of atmospheric contaminants by the resist film, since more contaminant absorbs in resists with PAB temperatures well below the bulk polymer T_g. It is interesting that the incomplete surface deprotection was observed in these PBOCSt / PFOS films. In spite of a significant excess of PFOS at the film surface, atmospheric contamination can still neutralize the excess surface acidity.

Surface Depth Profiling with NEXAFS

The electron yield signal is surface sensitive. By adjusting a negative voltage bias on the electron yield detector, different effective surface sampling depths can be probed. Figure 5 shows a schematic of the process. When the polymer film is excited by the incident X-ray radiation, the entire region of the film that absorbs photons also emits electrons. The electrons emitted deep within the film cannot escape. Only the electrons emitted near the top (1 to 8) nm from the film surface have enough energy to escape the surface potential. The electron yield detector has a grid where a negative voltage bias can be placed across the grid. The electrons that escape the surface of the film, but were emitted from furthest within the film will be low in energy due to inelastic interactions with other atoms. These low energy electrons will not have enough kinetic energy to pass the negative detector bias and will not be sensed. If the negative detector bias is gradually increased, progressively higher energy electrons are detected, and the effective electron yield sampling depth gets closer to the film surface.

We take advantage of this surface depth profiling capability in order to study the chemical composition profile of a model developed line edge region. Bilayer samples were made as described in the experimental section and elsewhere (4,5). Briefly, a layer of PBOCSt was spun on a silicon wafer. A second layer of PHS was spun on top of the PBOCSt. The PHS layer was also loaded with the photoacid generator, PFOS. The samples were exposed to UV radiation, post exposure baked (PEB) for various temperatures and times. During PEB, the acid diffuses into the PBOCSt underlayer, and initiates a diffusion / deprotection front that propagates into the underlayer. Finally, the films were developed in 0.26 N tetra-methyl-ammonium-hydroxide (TMAH) solution, which rinses away the top soluble portion of the film. We suspect that the breadth of the diffusion / reaction front in the line edge region will impact the development process and corresponding line edge roughness. Therefore it is important to develop techniques to measure the composition profile of the line edge region. We start by utilizing NEXAFS surface depth profiling on the model bilayer interfacial regions.

Figure 6 shows NEXAFS pre- and post-edge jump normalized spectra in the carbonyl absorption region, between (288 and 292) eV, for the bilayer samples after various PEB times at 90 ^{o}C and development in TMAH solution. For these NEXAFS spectra, the detector bias was fixed at –200 eV (sampling depth of roughly 30 Å, or three monomeric layers). Since the electron density of both PHS and PBOCSt are similar, fixing the detector bias essentially fixes the surface sampling volume. The top spectra is for the PBOCSt / PHS bilayer

without a PEB and after development in TMAH. In this sample, no deprotection occurs in the PBOCSt underlayer, and the carbonyl absorption is large. However, the carbonyl absorption clearly decreases with increasing bake temperatures, indicating that the extent of deprotection in the surface sampling volume is increasing. We propose that the decrease in the surface deprotection is due to broadening of the diffusion / reaction profile at short times leading to a broader surface composition profile in the developed bilayer. The surface composition is clearly changing over the sampling volume (roughly 30 Å at -200 eV detector bias), however, to prove that a broadening surface composition profile with increasing bake times, NEXAFS spectra must be taken as a function of the detector bias.

Figure 7 shows the NEXAFS spectra as a function of detector bias for a bilayer sample that was subjected to a short 15 s PEB at 90 ^{o}C. The spectra are both pre- and post-edge jump normalized so the carbonyl peak area represents the carbonyl group fraction in the sampling volume. As the negative detector bias increases, the effective electron yield sampling depth is progressively closer to the film surface (see schematic in Figure 7). The carbonyl peak area for this short PEB sample does not change dramatically with detector bias. This means that the composition does not change with the changing surface depth sampling volume, and indicates a very sharp surface composition profile over the total sampling volumes scanned with the various detector bias settings (see schematic in Figure 7).

Figure 8 shows the NEXAFS spectra as a function of detector bias for a bilayer sample that was subjected to a 60 s PEB at 90 ^{o}C. Again the spectra are both pre- and post-edge jump normalized. However, the carbonyl peak area decreases with increasing detector bias. Again, since the sampling area in the electron yield is progressively closer to the film surface with increasing detector bias, a decrease in the carbonyl peak area with increasing bias indicates a change in the surface composition and a broad composition profile over the sampling volumes scanned with the differing bias settings (see schematic in Figure 8). A comparison of the bias dependence of the carbonyl peak areas at 15 s (Figure 7) and 60 s (Figure 8) PEB times, qualitatively illustrates a broadening surface composition profile after development with increasing bake times. While the surface composition profile appears to broaden with time at short bake times, it is unclear at this time what transpires at longer bake times. It is also unclear how the breadth of the buried reaction / diffusion profile (before development) influences the corresponding dissolution process and the resulting surface composition profile and line edge roughness. While these areas are currently under investigation by a number of research groups, the development of high-resolution measurement capabilities allows the potential to make these connections. We are currently developing a theoretical formalism to quantitatively extract the surface composition profile from the NEXAFS bias dependant spectra.

Conclusions

With the advent of sub-100 nm lithography, interfacial phenomena will present significant problems for the resist performance. In order to understand and control the resist performance, it is necessary to have sensitive measurement capabilities that can elucidate the mechanisms causing common interfacial problems like t-topping, footing, undercutting, and line edge roughness. In this report, near edge X-ray absorption fine structure (NEXAFS) was utilized to probe interfacial chemistry in resist films. In particular, NEXAFS proved useful for qualitatively detecting segregation of a photoacid generator to the resist / air interface and differences in the deprotection reaction rate at that interface. In addition, by adjusting the bias on the electron yield detector, surface depth profiling capability of NEXAFS was demonstrated, qualitatively illustrating a broadening of the developed deprotection profile with bake times in a model line edge region. The depth profiling technique offers potential to provide insight into the mechanisms of the dissolution process and the relationship between the line edge chemistry and line edge roughness.

Acknowledgements

We gratefully acknowledge the support of the Defense Advanced Research Projects Agency Advanced Lithography Program under grant N66001-00-C-8803 and the NIST Office of Microelectronics Programs. J.L.L acknowledges support through the National Research Council-National Institute of Standards and Technology Postdoctoral Fellowship Program.

References

1. *2001 National Technology Roadmap for Semiconductors*, The Semiconductor Industry Association: San Jose, CA, (2001).
2. For detailed information about the NIST/Dow Soft X-ray Materials Characterization Facility at NSLS BNL, see: http://nslsweb.nsls.bnl.gov/nsls/pubs/newsletters/96-nov.pdf
3. D. A. Fischer, J. Colbert, J. L. Gland, Rev. Sci. Instrum. **60(7)**, 1596 (1989).
4. D. L. Goldfarb, M. Angelopoulos, E. K. Lin, R. L. Jones, C. L. Soles, J. L. Lenhart, W.-L. Wu, J. Vac Sci. Technol. B. **19(6)**, 2699 (2001).

5. E. K. Lin, C. L. Soles, D. L. Goldfarb, B. C. Trinque, S. D Burns, R. L. Jones, J. L. Lenhart, M. Angelopoulos, C. G. Willson, S. K. Satija, W.-L. Wu, Science, **297**, 372 (2002).
6. J. Stöhr, *NEXAFS Spectroscopy,* Springer Series in Surface Science (Springer, Heidelberg, 1992), Vol. 25.
7. O.Nalamasu, E. Reichmanis, J. E. Hanson, R. S. Kanga, L. A. Heimbrook, A. B. Emerson, F. A. Baiocchi, S. Vaidya, Poly. Eng. Sci. **32**, 1565 (1992).
8. S. A. MacDonald, W. D. Hinsberg, R. Wendt, N. J. Dlecak, G. C. Willson, C. D. Snyder, Chem. Mater. **5**, 348 (1993).
9. W. D. Hinsberg, S. A. MacDonald, N. J. Dlecak, C. D. Snyder, Chem. Mater. **6**, 481 (1994).
10. H. Yoshino, T. Itani, S. Hashimoto, M. Yamana, N. Samoto, K. Kasama, A. G. Timko, O. Nalamasu. Microelect. Eng. **35**, 153 (1997).

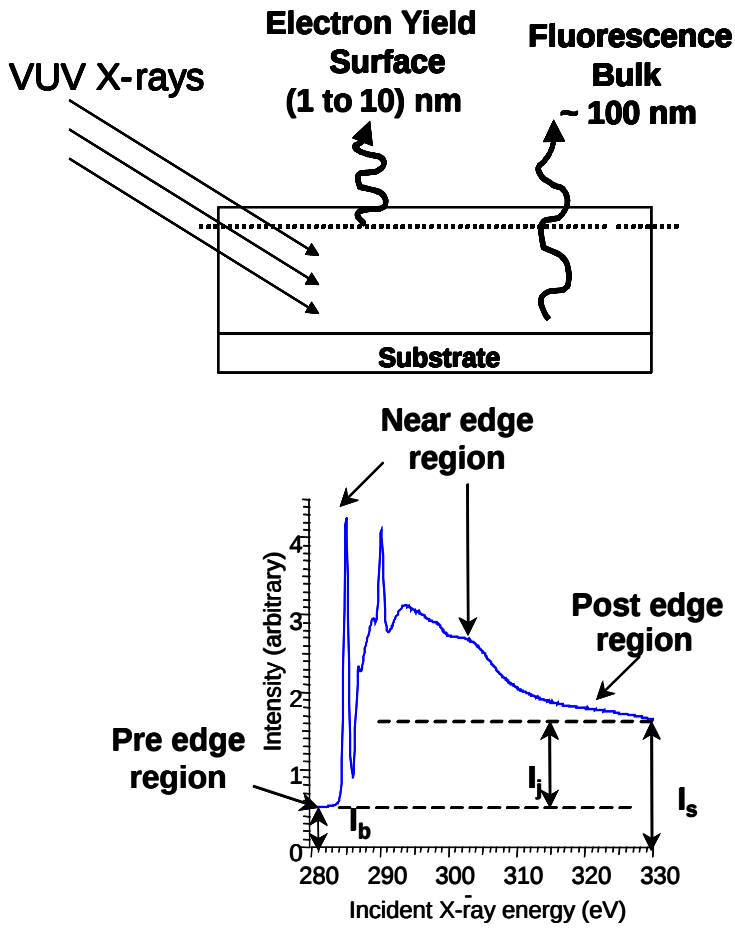

Figure 1. A schematic is shown of the NEXAFS experiment and typical spectra.

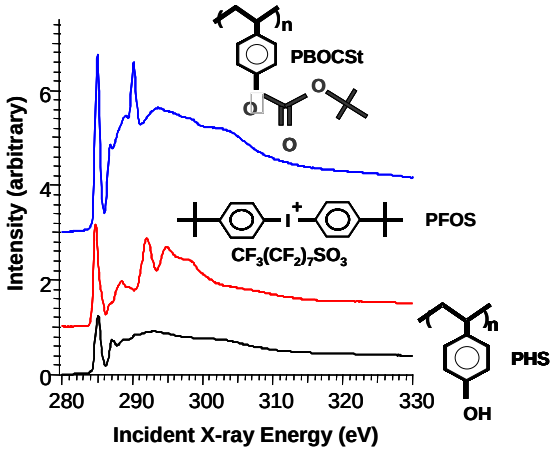

Figure 2. The electron yield NEXAFS spectra are shown for the pure resist components. The top is for PBOCSt. The middle is for PFOS. The bottom is for PHS.

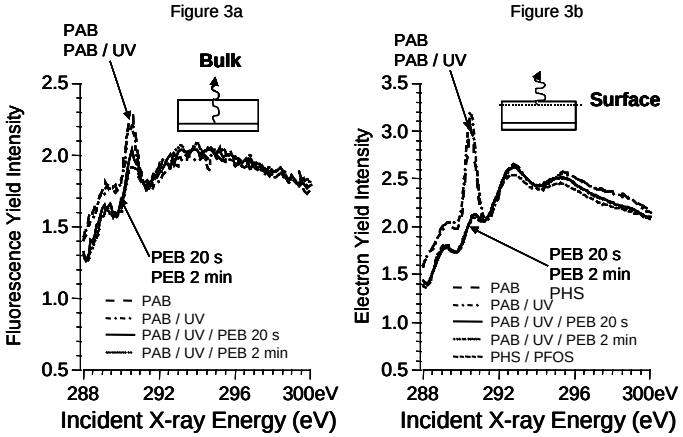

Figure 3. a) The fluorescence yield spectrum (bulk) is shown for the PBOCSt / PFOS films after different processing. b) The electron yield spectrum (surface) is shown for the same PBOCSt / PFOS films. Comparison of the electron and fluorescence yield shows that the surface reaction rate is faster than the bulk.

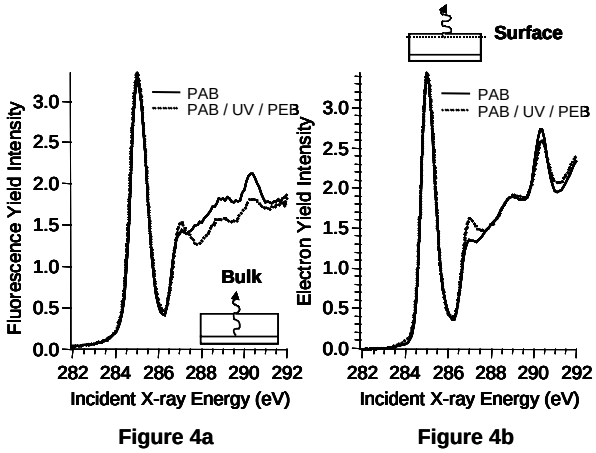

Figure 4. The carbon K-edge fluorescence yield spectra (Figure 4a), and carbon K-edge electron yield spectra (Figure 4b) are shown for the PBOCSt / PFOS film after PAB (solid line) and after UV exposure and a 2 min post exposure bake at 100 °C (dotted line). A post exposure delay of (5 to 10) min was incorporated in the processing.

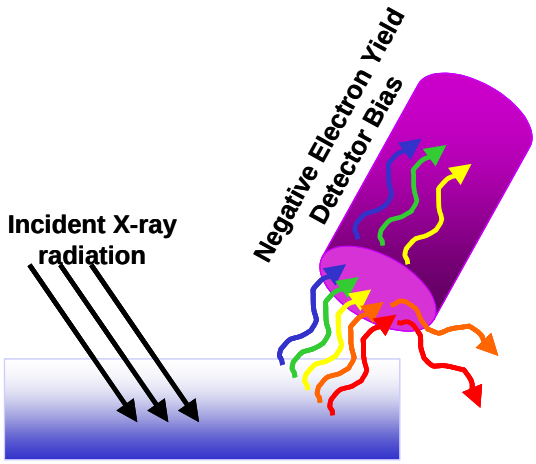

Figure 5. A schematic is shown of NEXAFS surface depth profiling.

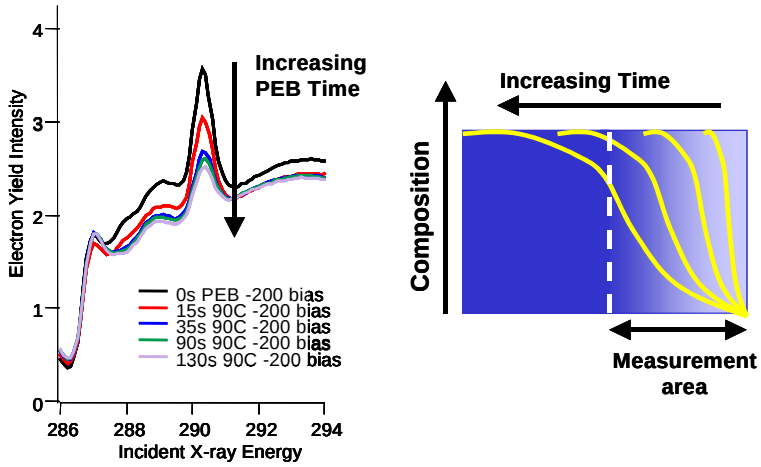

Figure 6. NEXAFS carbon edge electron yield spectra at a constant detector bias of –200 eV are shown for the developed bilayer samples with different PEB times at 90 °C.

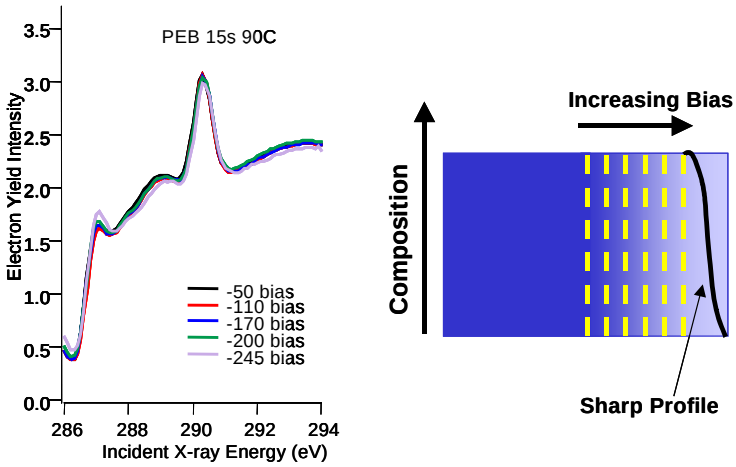

Figure 7. NEXAFS carbon edge electron yield spectra are shown as a function of detector bias for a bilayer with a 15 s PEB at 90 °C. The area of the carbonyl absorption does not change significantly with detector bias.

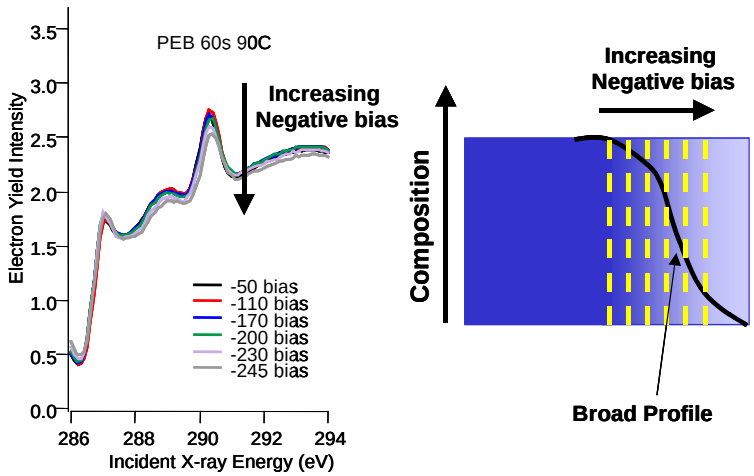

Figure 8. NEXAFS carbon edge electron yield spectra are shown as a function of detector bias for a bilayer with a 60 s PEB at 90 oC. The area of the carbonyl absorption decreases with increasing negative bias.